Turkish Journal of Electrical Engineering and Computer Sciences

Volume 30 | Number 5 Article 21

1-1-2022

Design and implementation of a bioinspired leaf shaped hybrid rectenna as a green energy manufacturing concept

KAYHAN ÇELİK

EROL KURT

Follow this and additional works at: https://journals.tubitak.gov.tr/elektrik

 Part of the Computer Engineering Commons, Computer Sciences Commons, and the Electrical and Computer Engineering Commons

Recommended Citation

ÇELİK, KAYHAN and KURT, EROL (2022) "Design and implementation of a bioinspired leaf shaped hybrid rectenna as a green energy manufacturing concept," *Turkish Journal of Electrical Engineering and Computer Sciences*: Vol. 30: No. 5, Article 21. https://doi.org/10.55730/1300-0632.3918
Available at: https://journals.tubitak.gov.tr/elektrik/vol30/iss5/21

This Article is brought to you for free and open access by TÜBİTAK Academic Journals. It has been accepted for inclusion in Turkish Journal of Electrical Engineering and Computer Sciences by an authorized editor of TÜBİTAK Academic Journals. For more information, please contact academic.publications@tubitak.gov.tr.

Turkish Journal of Electrical Engineering & Computer Sciences

http://journals.tubitak.gov.tr/elektrik/

Research Article

Turk J Elec Eng & Comp Sci
(2022) 30: 1995 – 2012
© TÜBİTAK
doi:10.55730/1300-0632.3918

Design and implementation of a bioinspired leaf shaped hybrid rectenna as a green energy manufacturing concept

Kayhan ÇELİK*, **Erol KURT**
Gazi University, Department of Electrical and Electronics Engineering, Faculty of Technology, Ankara, Turkey

Received: 29.12.2021 • **Accepted/Published Online:** 02.06.2022 • **Final Version:** 22.07.2022

Abstract: In this communication, the novel low cost hybrid energy harvester combining rectifying antenna with the solar cell for feeding the low power energy systems are reported. The bioinspired leaf shaped monopole antenna is designed to work in the most used communication frequency bands such as GSM-1800, UMTS-2100, WIFI-2.45 and LTE-2.65 GHz for the energy harvesting purposes and microstrip low pass filter is also added on the feeding line for the second harmonic rejection for increasing the efficiency of the harvester. The solar cell is placed on the ground plane of the designed leaf shaped antenna for using volumetric space efficiently and obtain a more compact system. The implemented prototype harvester generate 76 mV, 120 mV and 90 mV when the same type receiver antenna feed from the 25 dBm power from the RF source located at a distance of 1 m which satisfies the far field condition of the antenna without solar cell at the 2.15 GHz, 2.45 GHz and 2.65 GHz frequency bands, respectively. After the illumination of its solar cell component with 165 lux, the total harvested voltages are measured as 150 mV, 170 mV and 190 mV at the same frequency bands, respectively.

Key words: Broadband monopole antenna, solar cell, hibrid energy harvester, high frequency rectifier, low pass filter

1. Introduction

Today, global energy needs are increasing day by day due to reasons such as uncontrolled population growth, industrialization, increasing number of vehicles and heating needs due to increasing urbanization and increasing number of used tools with developing technology [1].

In parallel with the increase in energy requirements, the using of the fundamental energy sources (coal, oil and natural gas) are increasing. It is a scientific fact that fossil fuels will be exhausted in the next century due to the increasing energy need every day [2]. Due to the increase in the use of fossil fuels, the release of carbon derivatives released into the air are increasing and as a result of this, the natural balance deteriorates due to the global warming and various effects occur such as erosion, drought, floods and extinction of plant and animal species [3, 4]. In order to get rid of such negative effects and create a livable world for future generations, it is essential to use environmental and sustainable energy sources instead of fossil fuels. The solar and wind are the large-scale renewable energy sources which are the most used world widely and techniques for using efficiently these kind of energies are rather flourished in the last decades [5, 6]. However, the energy harvesting (EH) which means that capturing the small amount of low-scale ambient energies have a vital importance for the economy and the environment as well as the large-scale energy sources [7, 8].

*Correspondence: kayhancelik1923@gmail.com

This work is licensed under a Creative Commons Attribution 4.0 International License.

When the literature is examined, it is seen that the energy harvesting applications cover the very distinct energy sources and power levels from each other. In this context, mechanical energy [9, 10], light energy [11, 12], electromagnetic energy [13], thermal energy [14, 15] and wind energy [16, 17] can be given as a major topics [18]. With the advancing technology, energy harvesting applications find a place in many fields such as medicine, automotive and defense [19–21].

One of the significant reason for this is the economic and environmental contribution that occurs with the recycling of energy by the harvesting. The other important reason is that EH is a promising candidate for the powering of the low scale electronics systems such as wireless sensor networks since it is reality that these kind of systems are located to places physically difficult to access [22]. Because the harvesters provide the opportunity to operate without batteries, they allow many systems to work sustainably and uninterruptedly, in addition to this, they prevent the loss of time due to battery replacement as well as reducing the cost.

In this paper, low power hybrid energy harvester is proposed which one scavenges energy from electromagnetic waves and sun light simultaneously via the broadband antenna and the solar cell for obtaining more energy. The major motivation source when designing a novel broadband antenna is that the frequency bands used in the field of communication are expanded as a result of technological developments such as 3G, 4G, and 5G. In this manner, the presence of too many ambient electromagnetic waves in the environment allows them to be used as an energy source. Because of this, the novel bio-inspired leaf-shaped broadband antenna is designed to capture more electromagnetic waves through distinct frequency spectrum like GSM1800, UMTS Band 1, ISM Wi-Fi, and LTE Band 7, which ones satisfies the more energy than single channel systems [23–25]. The implemented harvester has the property of second harmonic rejection with an innovative antenna structure. The broadband half wave rectifier is also designed for converting the energy in all RF frequency bands to the DC electrical power with the help of the microstrip transmission lines and SMD circuit elements. In addition to the RF harvester, the solar cell is placed on the ground plane of the designed novel leaf shaped broadband antenna for saving space and to getting a modular and compact structure. The DC output ports of the each harvesters are connected in parallel to the load since the amount of power to be obtained at any time is expected to be greater than that of a single harvester. The hybrid system is modelled and analyzed via Ansys HFSS and Keysight ADS software, furthermore, their effects to each other are examined.

The remainder of paper is organized as follows: In Section 2, the detailed literature examination was given. In Section 3, the hybrid antenna was described in detail, along with its output as a function of bandwidth, gain, and radiation patterns. The rectifier and impedance matching units were defined in Section 4. The key findings from the theory and experiment were presented in Section 5. Finally, the major findings on the implemented harvester were expressed.

2. Literature review

The many broadband leaf-shaped bioinspired microstrip antennas have been presented by the antenna community in recent years. The rose leaf-shaped antenna with capacitive coupled rectangular fed [26], a maple leaf shaped UWB antenna [27], palmate leaf shaped antenna [28], the broadband CPW fed flower shaped antenna [29], castor leaf-shaped quasi-self-complementary antenna [30], a nature fern inspired fractal leaf structure planar antipodal Vivaldi antenna [31], Inga marginata leaf shaped antenna [32, 33], a leaf-shaped ultrawide band antenna [34–36], leaf shaped Koch fractal antenna [37], Carica Papaya leaf shaped antenna [38], Linden leaf shape antenna [39] are some of the important works in the literature.

When hybrid electromagnetic and solar energy harvesters are examined, one of the published early study

is done by Vaccaro [40]. In this study, for the aim of using in the satellite and terrestrial communications, the solar cells are placed into the ground plane of the slot antenna which one provides large metallic surface for the placing of the solar cell. The other important work is done by Collado [41, 42]. The broadband monopole rectenna is designed with the help of the low cost and flexible polyethylene terephthalate PET substrate and a flexible amorphous silicon solar cell which is placed inside the antenna for the applications of the energy autonomous low power wireless sensor networks and RFID. The other hybrid system consisting of a dual port rectangular slot antenna operates at 2.4 GHz ISM band, a 3D printed package, rectifier and power control unit, a solar cell, a microcontroller unit and RF transceiver is presented by Bito [43]. In this application, the solar cell is placed to the middle of the antenna for energy efficient internet-of-things wireless sensors. The other important work is that the design of a transparent multiport antenna integrated on the top surface of a solar cell for indoor applications. The advantage of this antenna is that it can capture much power due to multiport operation [44]. In addition to these tutorials, the more detailed information can be learned from the academic articles from the internet. The next section describes the designed novel antenna structure.

3. The concept of the hybrid antenna

That is a reality that with the increase in the number of frequency bands used in the communication industry, the amount of ambient energy in the environment will be much more. Accordingly, it is obvious that more energy from different frequency bands will be harvested with broadband antennas simultaneously. For this reason, it is an important point that the designed antenna should have the following features;

- It should be broadband to cover the one or more of the GSM communication frequencies simultaneously.
- Bandwidth of the antenna should be narrow enough to only cover RF frequencies so that the antenna could not be affected by high frequency harmonics generated by the diode which cause certain lose in the power.
- The radiation pattern of the antenna should be omnidirectional for capturing RF power from all directions regardless of antenna position.

In this respect, as the first step, it is decided to design the antenna as monopole since it provides broadband feature and omnidirectional radiation pattern [45–47]. The monopole antennas emerge as a suitable choice for broadband communication applications due to their large impedance bandwidths, nondirectional radiation patterns and their easy production with printed circuit technology [48]. When the literature is examined, it is seen that although there are many different monopole antenna designs, in reality these are generally in the form of derivatives of square, circular and triangular monopole antennas [49–55]. The reason why the monopole antenna operates as a wideband is that the ground plane at the backside does not cover the entire dielectric material since it has a finite-length ground plane. In this way, it supports more than one resonance mode at the same time and radiates broadbandly.

For this reason, the novel leaf shaped antenna (Antenna-1) given in Figure 1a has been designed at the first stage. In antenna design, FR-4 material with a dielectric coefficient of *4.4* and a tangent loss of *0.02* is preferred due to low cost and its abundance in the market. As seen from the figure, the antenna consists of leaf shaped radiating element and a microstrip transmission line for transmitting the electrical signal from the source to the radiation element on the front side. At the backside, it has a finite ground plane and there is a dielectric material between these two copper layers. All the parameter values of the antennas in Figure 1a, Figures 1b and 1c are given in Table 1. The leaf shape consists of *4* circles and *2* quarter arcs as given in Figure 2. The radius and center coordinates of the circles and arcs are given in Table 2. The maximum width and length of the leaf-shaped radiation element is nearly *34 mm*, *36 mm*, respectively. The width of the microstrip

transmission line which is used for feeding of the radiating element is calculated as *3 mm* which satisfies the characteristic impedance of *50 Ohm*. The length (l) of the Antenna-1 is calculated as:

$$l = R_1 + 6.8 + \sqrt{R_3^2 - 8.3^2} = 36 \quad mm \tag{1}$$

$$r = \frac{Designed \ \ antenna \ \ area}{2\pi l} = \frac{1025}{2 \ \pi \ 36} = 4.53 \quad mm \tag{2}$$

The fundamental design equation of the circular monopole antenna is given by [48, 56–58]:

$$f_L = \frac{7.2}{l + r + p} \quad GHz \tag{3}$$

In a given formula, the effective radius of an equivalent cylindrical monopole antenna, length of the monopole, the lower frequency of the antenna and the probe length are represented by the letter r, l, f_L and p, respectively, and given in cm. If the calculated values in Eqs. 1 and 2 are written in Eq. 3, the lower operating point of the suggested antenna system is calculated as:

$$f_L = \frac{7.2}{l + r + p} = \frac{7.2}{36 + 4.53 + 1} = 1.73 \quad GHz \tag{4}$$

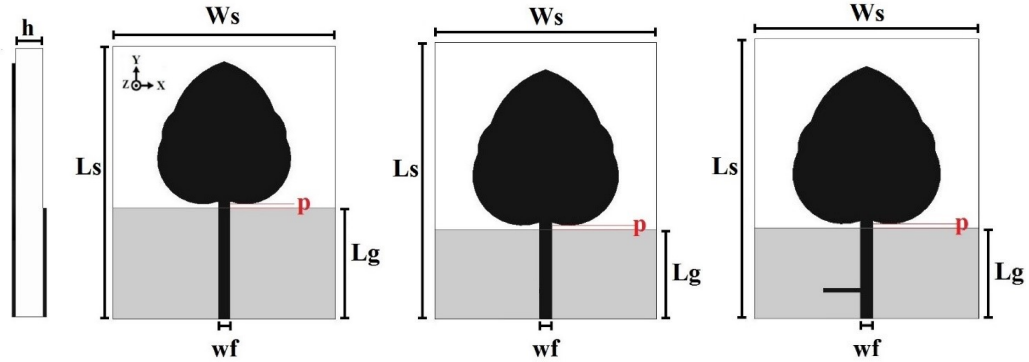


Figure 1. Design stages of proposed antenna.

Table 1. The parameter values of the Antennas.

Parameters (mm)	Ant. 1	Ant. 2	Ant. 3
W_s	57	52	52
L_s	70	65	65
L_g	28.5	21	21
w_f	3	3	3
h	1.6	1.6	1.6
p	1	1	1

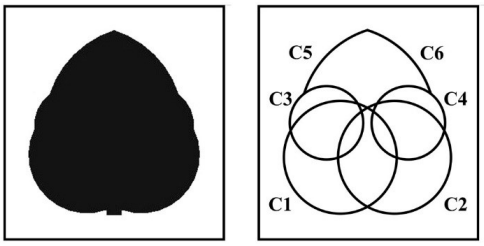


Figure 2. The forming of the leaf shape antenna.

Table 2. The center coordinates and radius values of the circles of the leaf shaped radiation element.

Circle	The center coordinates (x, y)	Radius (mm)
C1	–5.5, 35.7	11.7
C2	5.5, 35.7	11.7
C3	–8.3, 42.7	7.7
C4	8.3, 42.7	7.7
C5	–6, 42.7	20
C6	6, 42.7	20

The reflection coefficients of the antennas in Figure 1 are given in Figure 3. According to the simulated reflection coefficient of Antenna-1 in Figure 3, it can be concluded that, the lower operating frequency of the antenna is *1.6 GHz* and it is approximately the same as the calculated value. At the second step, the size of the ground plane of Antenna-1 and the length of the dielectric material are reduced in order to have a smaller antenna structure and Antenna-2 is obtained as seen from the Figure 1b. As a result of this process, reducing the size of the antenna does not cause a significant change in the reflection coefficient. However, as can be seen from the Figure 3, this antenna is also broadband and radiates at high frequencies (*f is greater than 3 GHz*), and it is undesirable situation since the frequency range to be used for RF energy harvesting is between *1.7 GHz* and *2.75 GHz*. Another negative aspect of this situation is that, it will cause the radiation of the waves at the *2nd* and *3rd* harmonic frequencies by the antenna which ones generated by the diode in the rectifier circuit and as a result, it will decrease the efficiency of the overall system. There are two ways to prevent this:

- Designing the antenna with band limited.
- Designing a low pass filter at the input port of the rectifier circuit.

Since designing a low-pass filter at the input port of the rectifier circuit increases the size of the circuit, 1st method is a more suitable solution. In order to achieve this and to change the antenna geometry for suppressing high frequencies, the current distribution of Antenna-2 is examined. The current distributions at different frequencies of Antenna-2 are given in Figure 4.

When the current distributions of Antenna-2 at the different frequencies are examined, it is seen that the current is concentrated on the microstrip feeding line and between the radiating element and the ground plane. It is especially concentrated on the feeding line at the *4 GHz* and above. Therefore, creating an additional current path on the feeding line will suppress the radiation at these frequencies. For this reason, in step 3, a single open stub transmission line is added on the feeding line as shown in Figure 1c. The width and length of this transmission line is *1 mm* and *8.5 mm*, respectively, and its distance to the feeding point is *6 mm*. The length of the stub is *0.227* λ_g in terms of wavelength at the *4.9 GHz* which is the *2nd* harmonic frequency of

2.45 GHz and it is approximately equal to *0.227* $\lambda_g/4$. The current distributions of Antenna-3 at the different frequencies is given in Figure 5. When figure is examined, it is observed that the current up to *3 GHz* is mostly concentrated between the upper side of the ground and the bottom side of the patch and above *3 GHz*, the current mostly flows over the stub. Figure 6 shows a comparison of the Antenna-3's simulated and measured reflection coefficients. According to the simulation, the operating frequency range of Antenna-3 is between *1.6 GHz* and *2.875 GHz* and has the bandwidth of *1.275 GHz*. However, the measured frequency range of the Antenna-3 is between *1.8 GHz* and *2.8 GHz* with the bandwidth of *1 GHz*. In general, it is seen that the reflection coefficient of the antenna has a similar trend as in the simulation, in addition to this; the bandwidth is also narrower than expected.

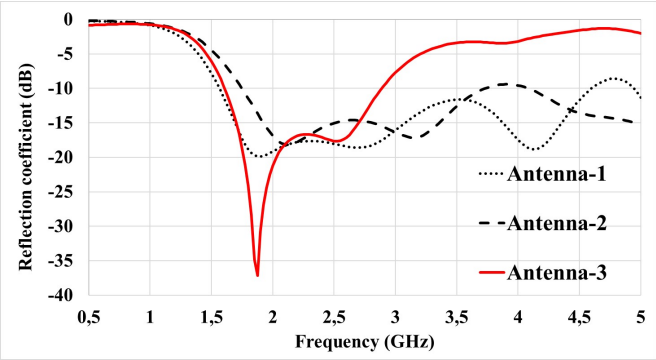
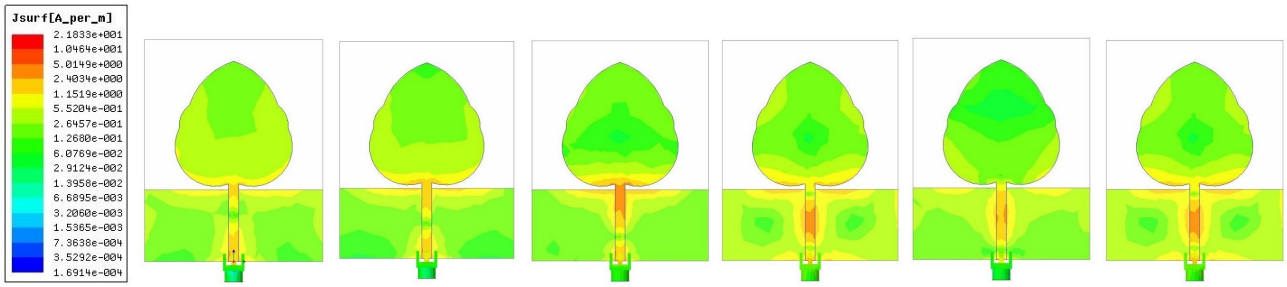
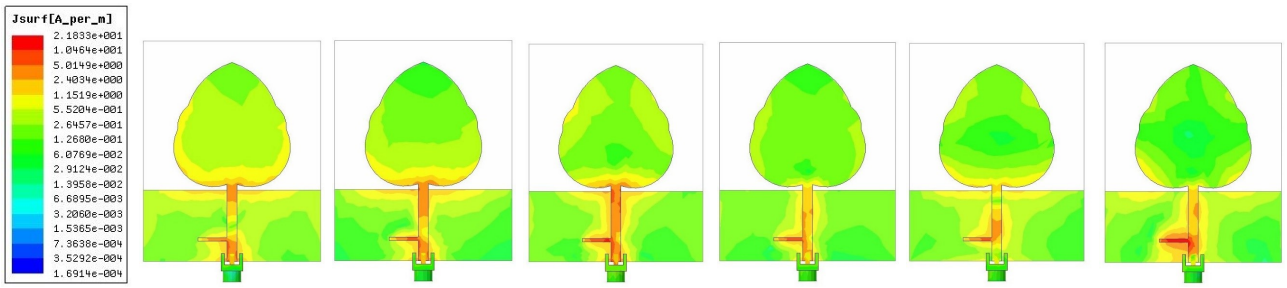


Figure 3. The reflection coefficients of the designed antennas.



(a) 2 GHz (b) 2.4 GHz (c) 3 GHz (d) 3.5 GHz (e) 4 GHz (f) 5 GHz

Figure 4. The current distributions of Antenna-2 at the different frequencies.



(a) 2 GHz (b) 2.4 GHz (c) 3 GHz (d) 3.5 GHz (e) 4 GHz (f) 5 GHz

Figure 5. The current distributions of Antenna-3 at the different frequencies.

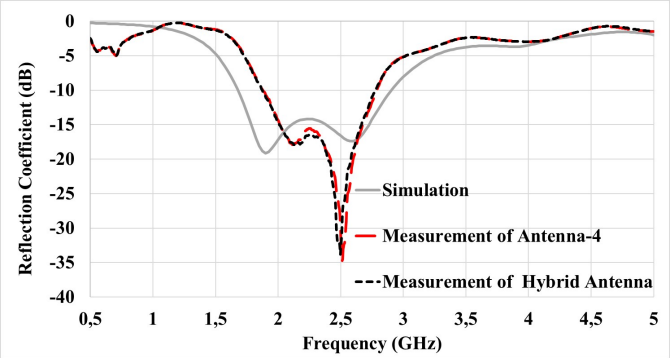
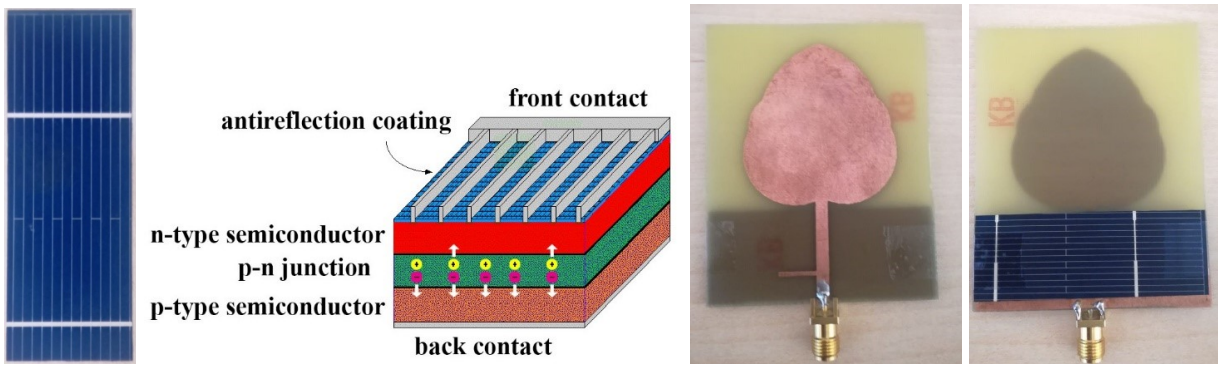


Figure 6. The simulated and measured reflection coefficients of Antenna-3 and hybrid antenna.

Finally, polycrystalline silicon solar cell is added to the ground plane of the designed antenna. The solar cell and its general structure are given in Figure 7. According to the figure it consist of the 3 layers; first one is the n-type and p-type semiconductor silicon materials which ones produce the electricity with the help of the sun. On the n-type silicon material, there is an antireflective surface to prevent the reflection of sunlight back into the atmosphere. Lastly, there are conductive aluminum contact points at the bottom and top of the cell for circuit connection. The open circuit voltage and short circuit current of solar cell are measured as *575 mV* and *180 mA*, respectively, when it is illuminated with *900* W/m^2 solar irradiance and the size of the cell is *52 x 19 x 0.2 mm*.

The most important layer in the structure of the cell that will affect the antenna performance is the silicon material, which constitutes the majority of the thickness of the cell, and its thickness varies between approximately *100-150* μm. The silicon layer with a thickness of about *0.15 mm* is equal to approximately 10% of the thickness of the dielectric material. Since the installation of the photovoltaic cell to the antenna ground plane will not significantly affect the effective dielectric constant of the antenna. Therefore, the antenna performance will not be affected by the photovoltaic cell. To prove this, the status of the antenna with and without solar cell is examined. The final version of the designed hybrid antenna is given in Figure 7.



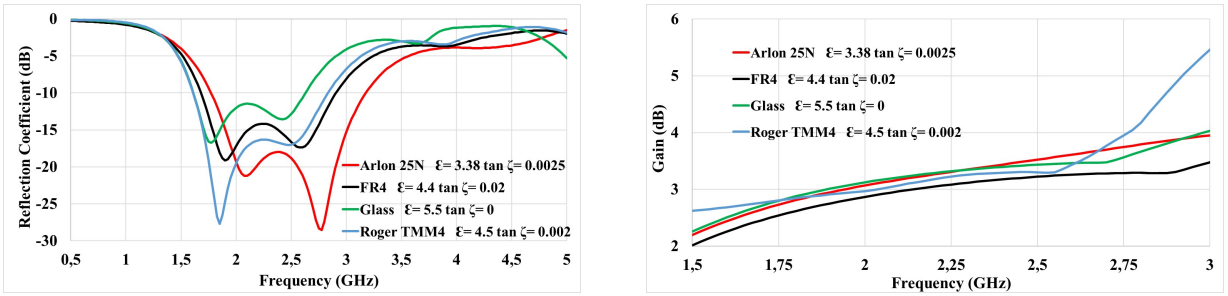
(a) The solar cell (b) The structure of the cell (c) Front view (d) Back view

Figure 7. Hybrid antenna.

The reflection coefficients and gain values of the antenna with the different dielectric materials are also examined and given in Figure 8, respectively. According to Figure 8a, it is seen that the lower cut-off frequencies are the same (1.625 GHz) in the designs made with Glass and Roger TMM4. The lower cutoff frequencies of

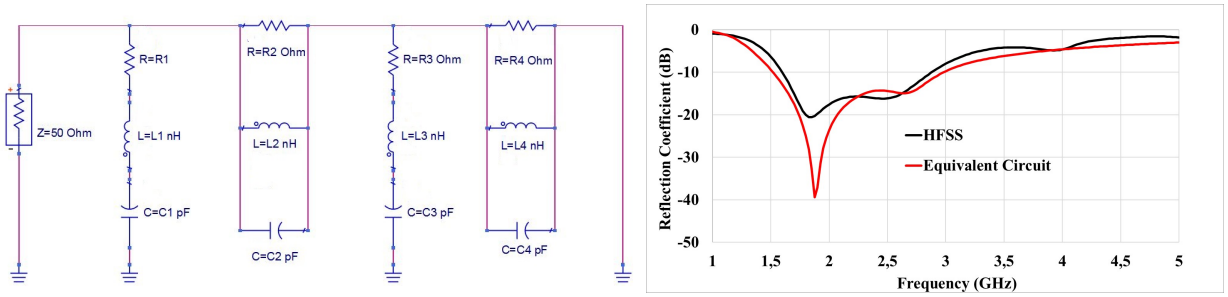
the FR4 and Arlon 25N are 1.675 GHz and 1.8 GHz, respectively. The upper cutoff frequencies of the materials from low to high are Glass (2.625 GHz), Roger (2.825 GHz), FR4(2.9 GHz) and Arlon (3.175 GHz), respectively. According to these values, the material with the largest bandwidth is Arlon 25N (1.375 GHz) and the material with the smallest bandwidth is Glass (1 GHz). The bandwidths of Roger and FR4 are almost the same, with 1.2 GHz and 1.225 GHz.

The gain values for the simulations of the designed antenna using the above-mentioned materials are given in Figure 8b. When the figure is examined, it is seen that the gain value of FR4 is smaller than the others in the interested frequency band. It is seen that gains of Glass and Arlon are almost the same and Roger has a gain value of lower than these. The approximate equivalent circuit model of the designed antenna and the comparison of reflection coefficients obtained from antenna equivalent circuit and antenna simulation are given in Figures 9a and 9b, respectively.



a) The reflection coefficients b) Gain

Figure 8. The designed antenna with different dielectric materials.



a) The equivalent circuit of the antenna b)The reflection coefficients

Figure 9. The comparison of reflection coefficients of antenna and equivalent circuit.

The reflection coefficients of Antenna-3 and hybrid antenna is also given in Figure 6. It is clear that, adding the photovoltaic cell to the antenna does not have any negative effect on the reflection coefficient. The radiation patterns and gain measurement of the antennas in the anechoic chamber is shown in Figure 10. The measured radiation patterns of hybrid antenna at different frequencies are given in Figure 11. According to Figure 11, it is seen that the designed antenna has an omnidirectional radiation pattern at the *X-Z (phi = 0)* plane at the all interested frequency bands. In addition to this, the antenna has a linear polarization characteristic. The comparison of the gain values of antenna with and without the solar cell depending on the frequency are given in Figure 12. When the figure is examined, it is seen that both antennas generally have a similar gain trend and it is observed that the maximum gain values are almost equal to each other, but there

are differences in some frequency bands. It is seen that there is approximately *1 dB* reduction in the gain of the antenna with solar cell at the *1.5 GHz* frequency band. In the *1.5–1.7 GHz* frequency range, the gain of the antenna with solar cell increases and reaches the maximum value of *4.2 dB* at *1.7 GHz*. In the *1.75–2.1 GHz* frequency band, it is seen that the gain of the antenna with solar cell decreases, while the antenna without solar cell follows a horizontal line in this region. In the range of *2.1–2.2 GHz*, there is an increase in the gain of the antenna with solar cell again, and it follows a horizontal trend between *2.2–2.45 GHz* range. It appears that the gains of the both antennas are almost the same at the *2.45 GHz* and *2.65 GHz* bands. After the *2.65 GHz* band, the gain of the antenna with solar cell follows a horizontal trend, and in addition to this, the gain of the antenna without solar cell decreases dramatically.

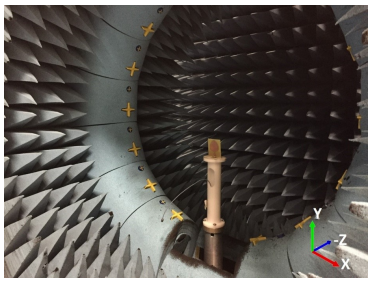


Figure 10. The setup of the radiation pattern measurement.

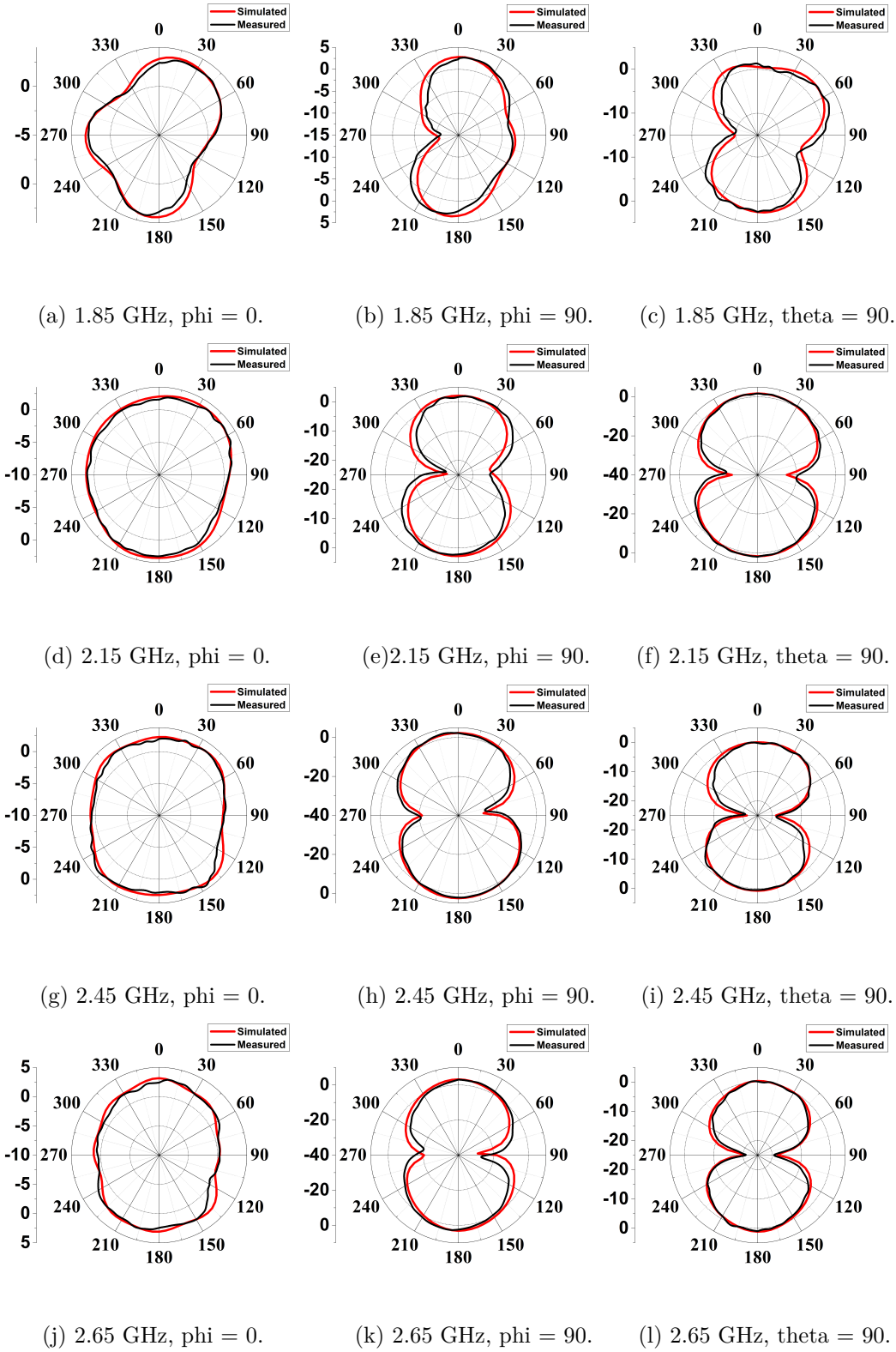
The comparison chart of the leaf–shaped antenna with the identical ones in the antenna community is presented in Table 3. The measured operating frequency range of the designed antenna is from 1.8 GHz to 2.8 GHz. When the table is examined, the implemented antenna has the smallest fractional bandwidth. The key explanation of this situation can be given as the design is equipped RF-EH applications running on less than 3 GHz. The proposed hybrid antenna has a higher gain values than Refs. [26, 29–31, 34, 35, 37] at expressed low frequency values. In addition this, Refs. [27, 28, 36, 38] have a higher gain values then the presented one.

4. Designing of the rectifier

It can be seen when scholarly papers are reviewed that different rectifier structures are implemented for DC power generation from the AC signals. In that context, single series [59], single shunt [60], differential rectifier [61], voltage doubler [22] and Greinacher charge pump [62] can be given as a tutorial. Due to the low level of ambient electromagnetic power in the environment, the construct of a rectifier unit for working efficiently at low power levels such as *-15 dBm* is considered in the present work. Another design parameter is that proposed rectifier should be able to work simultaneously and effectively at more than one RF frequency bands. In the some academic studies, it is shown that the efficiency of a half-wave rectifier is much more than voltage doubler and Greinacher charge pump [63]. Because of this, the half wave rectifier circuit topology is selected as an AC to DC converter.

The general topology of the hibrid electromagnetic and solar harvester with the rectifier circuit and impedance matching circuit is given in Figure 13. The circuit is operating at *1.85 GHz*, *2.15 GHz*, *2.45 GHz* and *2.65 GHz* bands with the different efficiency values and designed by using Skyworks SMS7630-079 Schottky diodes, *Murata Electronics GRM21B7U1A104JA01L 100 nF* capacitor, *Coilcraft 0805CS 5.6 nH* and *68 nH* inductors with the optimum load value of *1700 Ohm*.

Implementing a broadband impedance matching is not an easy task since the impedance of the rectifier circuit changes depending on the frequency, input power, diode impedance and load resistance. Because of this,



(a) 1.85 GHz, phi = 0. (b) 1.85 GHz, phi = 90. (c) 1.85 GHz, theta = 90.

(d) 2.15 GHz, phi = 0. (e)2.15 GHz, phi = 90. (f) 2.15 GHz, theta = 90.

(g) 2.45 GHz, phi = 0. (h) 2.45 GHz, phi = 90. (i) 2.45 GHz, theta = 90.

(j) 2.65 GHz, phi = 0. (k) 2.65 GHz, phi = 90. (l) 2.65 GHz, theta = 90.

Figure 11. The radiation patterns of the hybrid antenna at different frequencies.

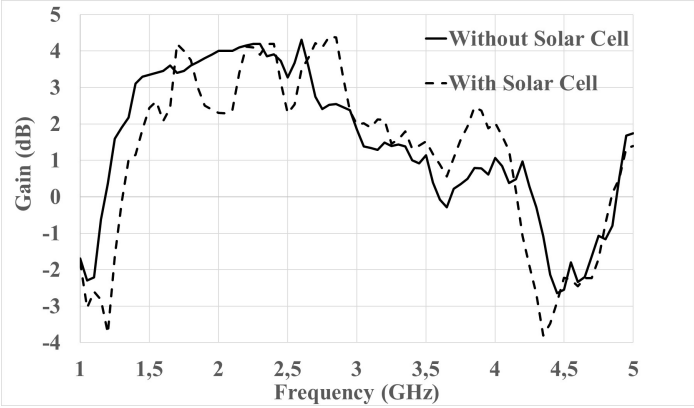


Figure 12. The measured gain of the designed antenna versus frequency.

Table 3. The comparison chart of the antennas.

Reference	Bandwidth (GHz) S11 < -10dB	Fractional Bandwidth (%)	Size (mm) W x L x h	Gain (dBi)
[26]	4.3–8.36	64.14	100 × 100 × 8	1.6 @ 4 GHz
[27]	3.1–13.15	123.7	30.5 × 35.5 × 1.58	9 @ 3 GHz
[28]	3.08–14.38	129.4	13.5 × 14.8 × 0.8	Nearly 4 @ 3 GHz
[29]	2.2–10.6	131.25	28 × 41.8 × 1.6	Nearly 2.5 @ 3 GHz
[30]	2.2–13	142.1	32.4 × 40 × 0.8	Nearly 2.5 @ 2.5 GHz
[31]	1.3–20	175.6	50.8 × 62 × 0.8	Nearly 2 @ 2.5 GHz
[32]	2.74–13	130.4	45 × 30 × 1.5	3.84 @ 3.2 GHz
[34]	3.1–10.6	111.9	38.31 × 34.52 × 0.8	Nearly 2.3 @ 2.5 GHz
[35]	2.58–11.62	127.3	38.31 × 34.52 × 0.8	Nearly 2.3 @ 2.5 GHz
[36]	3–14.64	131.08	40 × 30 × 0.8	Nearly 5 @ 2.5 GHz
[37]	1.977, 3.19, 6.32 8.814, 11.87, 15.69 and 18.3	-	14 x 16 x 1.6	Nearly 3 @ 3 GHz
[38]	1.9–6.2 6.99–7.44 9.15–9.35	106.17 6.23 1.08	59.25 x 35.7 x 1.58	8.94 @ 2.1 GHz 12.5 @ 2.5 GHz
Present work	1.8-2.8	43.48	52 x 65 x 1.6	3 @ 1.85 GHz 3.4 @ 2.15 GHz 3.14 @ 2.45 GHz 3.81 @ 2.65 GHz

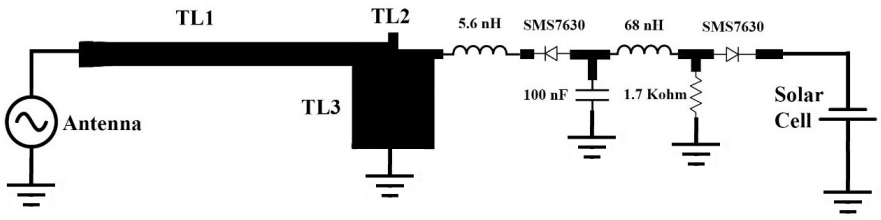


Figure 13. The multiband hybrid energy harvester topology.

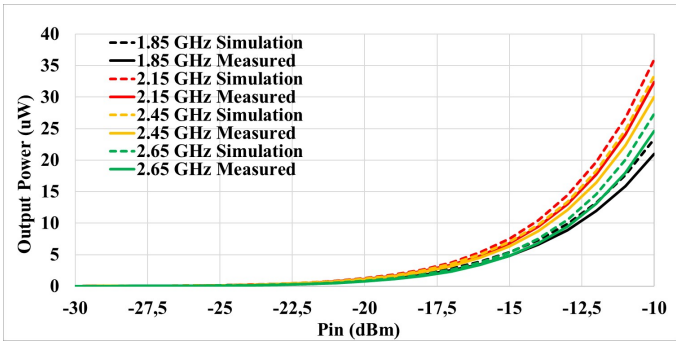


Figure 14. The simulated and measured power values of the rectifier circuit.

the impedance matching circuit of the rectifier is simply realized with a single-stub impedance matching circuit and a serial transmission line in order to maximize the output DC power of the system as much as possible.

The main purpose of the using single short stub which one has an admittance value characterized with Eq. 5 is to eliminate the admittance of the rectifier as much as possible in the interested frequency bands. In addition to this, the open circuit stub has a little effect on the eliminating of the rectifier admittance. And lastly, the single series transmission line with the 50 Ohm characteristics impedance is added for the increasing the impedance matching of the of the system.

$$Y_s(f) = \frac{1}{jZ_s tan\theta_s(f)} \tag{5}$$

Table 4 shows the *length (L)* and *width (W)* of the transmission lines in the rectifier unit. The ADS software is used to analyze and optimize the rectifier block which was made on a *1.6 mm* FR4 circuit board with a dielectric constant of *4.4* and a loss tangent of *0.02*. The operation of the rectifier was simulated and measured according to different input power values from *-30 dBm* to *-10 dBm* and output power and efficiency graphics are given separately in Figures 14 and 15.

Table 4. The parameter values of the circuit.

Parameters	Value (mm)
TL1 (Width)	3
TL1 (Length)	30.2
TL2 (Width)	1
TL2 (Length)	1
TL3 (Width)	9.4
TL3 (Length)	9.4

According to Figure 14, the output power is increasing with the input power exponentially. Power values at different frequencies have an almost similar graph and it was observed that the difference between them increases as the enhancing of the input power level. The minimum power value was measured at *-30 dBm* input value at the frequency of *2.65 GHz* nearly *13 nW*. The power values at other frequencies are *13*, *12* and *9 nW*, respectively, at *1.85 GHz*, *2.15 GHz* and *2.45 GHz*. The maximum power value was measured at the *-10 dBm* input value at the frequency of *2.15 GHz* as *32 uW*. The other power values at this input level are *21 uW*, *30 uW* and *24 uW* at *1.85 GHz*, *2.45 GHz* and *2.65 GHz*, respectively.

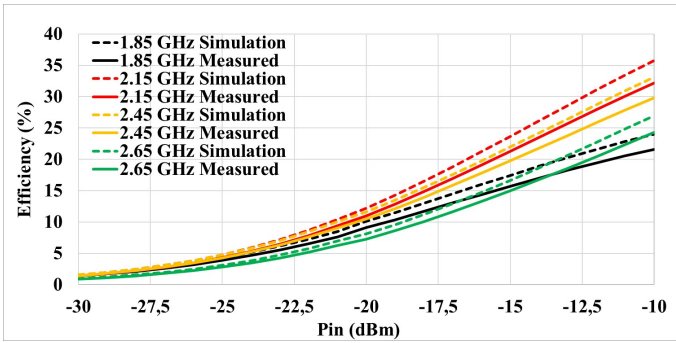


Figure 15. The simulated and measured efficiency values of the rectifier circuit.

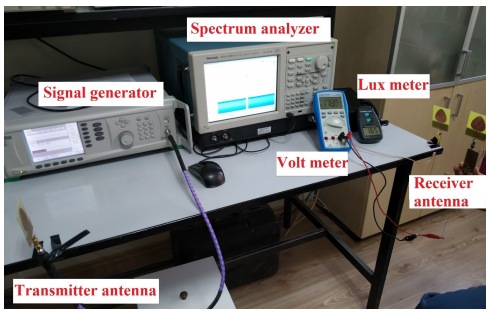


Figure 16. Real time measurement of the designed hybrid energy harvester at indoor environment.

In terms of efficiency, in Figure 15, the measured minimum values are *1.3%, 1.3%, 1.2%* and *0.9%* at *1.85 GHz*, *2.15 GHz 2.45 GHz* and *2.65 GHz* bands, respectively, at the *-30 dBm* input power. In addition to this, the maximum efficiencies were measured at *-10 dBm* with the *21.6%, 32.2 %, 29.8 %, 24.2 %* , respectively. The efficiency graphs also follow a similar trend as a power graphs and the efficiency values are increasing with the increasing of power level.

5. Results and discussion

Table 5 also includes the comparison of the designed rectenna in terms of the performance with close examples found in the academic community. In the table, apart from Ref. [64], all of the rectenna systems' RF input powers are identical and the value of it is higher than others as *-10 dBm*. In spite of this, Ref. [44] has the maximum efficiency value with the *28.6 %*. The main reason for this is the used antenna system has a multiport input, so that, the total power entering the system is high since energy is taken from more than one channel at the same time. Ref. [42] has the second biggest efficiency value with the *15 %* and this value is followed by Ref. [43] with *11 %*. The proposed system has the efficiency values between the *7 %* and nearly *11 %* at *-20 dBm*. The reason for the low efficiencies is that a wide-band impedance matching could not be made since impedance of the diode and other lumped elements change according to the frequency. On the other hand, since the sizes of solar cells and the amount of light received by the cells are different; it is not very convenient to compare the power obtained from the solar cells.

In addition to this, the performance of the hybrid rectenna system is tested in real time indoor environment as seen from Figure 16. The rectenna system is powered by the fabricated same antenna which acts as a transmitter antenna connected to Anritsu MG3692C signal generator with the input power level of *25 dBm (0.316 W)*. The receiver hybrid rectenna is located nearly *100 cm* away from the transmitter for providing the

Table 5. Performance comparison of the rectenna.

Reference	[42]	[43]	[44]	[64]	Present work
Energy source	EM / Light	EM / Light	EM / Light	EM / Light	EM / Light
Antenna frequency	850 MHz 1850 MHz	2.28–2.55 GHz	2.38–2.5 GHz	2.3–2.45 GHz	1.85 GHz 2.15 GHz 2.45 GHz 2.65 GHz
Area of solar cell (mm^2)	N.A.	22.8 × 24	150 × 150	N.A.	52 × 19
Area of the antenna (mm^2)	N.A.	45 × 45	150 × 150	N.A.	52 × 65
Maximum gain	2.23 dBi	7.4 dBi	5 dBi	1.9 dBi	4.3 dBi
Output of the solar power	56 mW @ 1000W/ m^2 and –20 dBm	70.5 uW @ 334 lux	1.68 mW @ 360 lux	<0.75 mW @ 10 W / m^2	11.65 uW @ 165 lux
Output of the RF power		–10 dBm input 35 uW @ 2.45 GHz	0.34 mW @ 2.45 GHz	–10 dBm input <0.02 mW @ 2.45 GHz	5.35 uW (average at single band)
RF efficiency	15 % @ –20 dBm	Nearly 11 % @ –20 dBm	28 % @ –20 dBm	10 % @ –10 dBm	9.2%, 1.85 GHz 10%, 2.15 GHz 11%, 2.45 GHz 7%, 2.65 GHz @–20 dBm

far field condition. A second antenna with the same characteristics is connected to the Tektronix RSA5126B Spectrum Analyzer for calculating the receiver antenna's input power level. The lux meter is used to measure the light intensity in the indoor environment. As a result of the measurements, it has been observed that the receiver antenna has an output voltages of *76 mV*, *120 mV*, and *90 mV*, respectively, at the frequency bands of *2.15 GHz*, *2.45 GHz*, and *2.65 GHz*, respectively. When the solar cell is activated, under the same conditions with *165 lux* light intensity, output voltages of *150 mV*, *170 mV*, and *190 mV* are obtained in the same frequency bands, respectively. Since the signal generator does not generate a signal below *2 GHz*, the values at *1.8 GHz* could not be measured. The results obtained show that the designed system can be used to feed low power sensor networks and microelectronic systems.

6. Conclusion

In this communication, the multiband hybrid electromagnetic and solar energy harvester is designed and implemented for the low level of powers in the ambient environment. Firstly, a unique bioinspired hybrid antenna with the harmonic rejection characteristic is clarified. The design variables are described and performance parameters such as bandwidth and gain graphs are presented. At the AC to DC converter stage, design and the working state of the multiband-half wave rectifier is given in details. Because the amount of ambient electromagnetic energy is low in real-world conditions, the rectifier is customized according to this situation. The designed hybrid harvester produce the voltage level between the 76–90 mV without the solar cell and harvests the voltage level between the 150–190 mV with the solar cell. The output average powers are nearly 5.35 uW and 17 uW without and with the solar cell, respectively. As a result, the measurements prove that

multiband hybrid rectenna operate efficiently at the low-level powers at the real environment and it can be used as a battery source for the low scale electronic systems.

Acknowledgment

This study was supported by Gazi University Scientific Research Projects Unit (BAP). (Project No: 07/2020-03).

References

[1] Lv J, Li YP, Shan BG, Jin SW, Suo C. Planning energy-water nexus system under multiple uncertainties–A case study of Hebei province. Applied Energy 2018; 229:389-403. doi:10.1016/j.apenergy.2018.08.010

[2] Tabakaev R, Shanenkov I, Kazakov A, Zavorin A. Thermal processing of biomass into high-calorific solid composite fuel. Journal of analytical and applied pyrolysis 2017;124:94-102. doi:10.1016/j.jaap.2017.02.016

[3] Jackson RB, Friedlingstein P, Andrew RM, Canadell JG, Le Quéré C et al. Persistent fossil fuel growth threatens the Paris Agreement and planetary health. Environmental Research Letters 2019; 14 (12) : 121001. doi:10.1088/1748-9326/ab57b3

[4] Annamalai K, Thanapal SS, Ranjan D. Ranking renewable and fossil fuels on global warming potential using respiratory quotient concept. Journal of Combustion 2018. doi:10.1155/2018/1270708

[5] Boddapati, V., Nandikatti, A.S., and Daniel, S.A., Design and feasibility analysis of a solar PV array installation during the construction of high-rise residential buildings. Journal of Energy Systems 2021; 5(2) :60-79, DOI: 10.30521/jes.811978

[6] Ali, I, A., and Elshafei, A. L., Model predictive control stabilization of a power system including a wind power plant. Journal of Energy Systems 2022; 6(2) :188-208, DOI: 10.30521/jes.997307

[7] Crepaldi M, Grosso M, Sassone A, Gallinaro S, Rinaudo S et al. A top-down constraint-driven methodology for smart system design. IEEE Circuits and Systems Magazine 2014; 14 (1) :37-57. doi:10.1109/MCAS.2013.2296415

[8] Mutlu, B., Kurt, E., Bizon, N. and Lopez Guede J.M. Design and Fabrication of a New Micro-Power Scaled Electromagnetic Harvester, Journal of Energy Systems 2019; 3(2) :51-66, doi: 10.30521/jes.554900

[9] Debnath B, Kumar R, Shakeel PM. Meandering-trapezoidal shaped MEMS structure for low frequency vibration based energy harvesting applications. Sustainable Energy Technologies and Assessments 2020; 42:100881. doi:10.1016/j.seta.2020.100881

[10] Zhou M, Al-Furjan MSH, Zou J, Liu W. A review on heat and mechanical energy harvesting from human–Principles, prototypes and perspectives. Renewable and Sustainable Energy Reviews 2018 ; 82: 3582-3609. doi:10.1016/j.rser.2017.10.102

[11] Bhalla V, Tyagi H. Solar energy harvesting by cobalt oxide nanoparticles, a Nano fluid absorption based system. Sustainable Energy Technologies and Assessments 2017; 24: 45—54. doi:10.1016/j.seta.2017.01.011

[12] Lechêne BP, Cowell M, Pierre A, Evans JW, Wright PK et al. Organic solar cells and fully printed super-capacitors optimized for indoor light energy harvesting. Nano Energy 2016; 26: 631-640. doi:10.1016/j.nanoen.2016.06.017

[13] Çelik K, Kurt E. A novel meander line integrated E-shaped rectenna for energy harvesting applications. International Journal of RF and Microwave Computer-Aided Engineering 2019; 29 (1): e21627. doi:10.1002/mmce.21627

[14] Sheehan DP, Welsh TM. Epicatalytic thermal diode: Harvesting ambient thermal energy. Sustainable Energy Technologies and Assessments 2019; 31: 355-368. doi:10.1016/j.seta.2018.11.007

[15] Kishore RA, Priya S. A review on low-grade thermal energy harvesting: materials, methods and devices. Materials 2018; 11 (8):1433. doi:10.3390/ma11081433

[16] Shaltout ML, Yan Z, Palejiya D, Chen D. Tradeoff analysis of energy harvesting and noise emission for distributed wind turbines. Sustainable Energy Technologies and Assessments 2015; 10:12-21. doi:10.1016/j.seta.2015.01.005

[17] Jahangir MH, Cheraghi R. Economic and environmental assessment of solar-wind-biomass hybrid renewable energy system supplying rural settlement load. Sustainable Energy Technologies and Assessments 2020; 42:100895. doi:10.1016/j.seta.2020.100895

[18] Eyüboğlu, D. K., A General Survey on the Wireless Power Transfer. Transactions On Electromagnetic Spectrum, 2022; 1(1), 10–13. https://doi.org/10.5281/zenodo.6644922

[19] Stopjakova V, Kovac M, Potocny M. On-Chip Energy Harvesting for Implantable Medical Devices. Radioengineering 2020; 29 (2): 269. doi:10.13164/re.2020.0269

[20] Abdelkareem MA, Xu L, Ali MKA, Elagouz A, Mi J et al. Vibration energy harvesting in automotive suspension system: A detailed review. Applied energy 2018; 229:672—699. doi:10.1016/j.apenergy.2018.08.030

[21] Balraj S, Ganesan A. Indirect Rotational Energy Harvesting System to Enhance the Power Supply of the Quadcopter. Defence Science Journal 2020; 70 (2). doi:10.14429/dsj.70.14568

[22] Nie MJ, Yang XX, Tan GN, Han B. A compact 2.45-GHz broadband rectenna using grounded coplanar waveguide. IEEE antennas and wireless propagation letters 2015; 14: 986—989. doi:10.1109/LAWP.2015.2388789

[23] Selvan S, Zaman M, Gobbi R, Wong HY. Recent advances in the design and development of radio frequency-based energy harvester for powering wireless sensors: a review. Journal of Electromagnetic Waves and Applications 2018; 32 (16): 2110—2134. doi:10.1080/09205071.2018.1497548

[24] Khemar A, Kacha A, Takhedmit H, Abib G. Design and experiments of a dual-band rectenna for ambient RF energy harvesting in urban environments. IET Microwaves, Antennas & Propagation 2018; 12 (1): 49—55. doi:10.1049/iet-map.2016.1040

[25] Niotaki K, Kim S, Jeong S, Collado A, Georgiadis A et al. A compact dual-band rectenna using slot-loaded dual band folded dipole antenna. IEEE Antennas and Wireless Propagation Letters 2013; 12:1634—1637. doi:10.1109/LAWP.2013.2294200

[26] Lotfi N, Abbas A. Ultra wideband rose leaf microstrip patch antenna. Progress In Electromagnetics Research 2018; 86 :155—168. doi:10.2528/PIER08090201

[27] Ahmed OMH, Sebak A. A novel maple-leaf shaped UWB antenna with a 5.0-6.0 GHz band-notch characteristic. Progress In Electromagnetics Research 2009; 11:39—49. doi:10.2528/PIERC09091107

[28] Fakharian MM, Rezaei P. Very compact palmate leaf-shaped CPW-FED monopole antenna for UWB applications. Microwave and Optical Technology Letters 2014; 56 (7): 1612—1616. doi:10.1002/mop.28395

[29] Patre SR, Singh SP. CPW-fed flower-shaped patch antenna for broadband applications. Microwave and Optical Technology Letters 2015; 57 (12): 2908—2913. doi:10.1002/mop.29480

[30] Patre SR, Singh SP. Castor leaf-shaped quasi-self-complementary antenna for broadband applications. 2015 International Conference on Microwave and Photonics (ICMAP); Dhanbad, India;2015. pp.1-2. doi:10.1109/ICMAP.2015.7408782

[31] Biswas B, Ghatak R, Poddar DR. A fern fractal leaf inspired wideband antipodal Vivaldi antenna for microwave imaging system. IEEE Transactions on Antennas and Propagation 2017; 65 (11) :6126-6129. doi:10.1109/TAP.2017.2748361

[32] Cruz JDN, Freire RCS, Serres AJR, Moura LCMD, Costa APD et al. Parametric study of printed monopole antenna bioinspired on the Inga Marginata leaves for UWB applications. Journal of Microwaves, Optoelectronics and Electromagnetic Applications 2017; 16 (1): 312—322. doi:10.1590/2179-10742017v16i1891

[33] Cruz JDN, Serres AJR, de Oliveira AC, Xavier GVR, de Albuquerque CCR et al. Bio-inspired printed monopole antenna applied to partial discharge detection. Sensors 2019; 19 (3): 628. doi:10.3390/s19030628

[34] Kundu S, Jana SK. A leaf-shaped CPW-fed UWB antenna for GPR applications. Microwave and Optical Technology Letters 2018; 60 (4): 941—945. doi:10.1002/mop.31089

[35] Kundu S, Jana SK. Leaf-shaped CPW-fed UWB antenna with triple notch bands for ground penetrating radar applications. Microwave and Optical Technology Letters 2018; 60 (4): 930—936. doi:10.1002/mop.31075

[36] Kundu S, Chatterjee A, Jana SK, Parui SK. Gain enhancement of a printed leaf shaped UWB antenna using dual FSS layers and experimental study for ground coupling GPR applications. Microwave and Optical Technology Letters 2018; 60 (6): 1417—1423. doi:10.1002/mop.31171

[37] Elavarasi C, Shanmuganantham T. Multiband SRR loaded leaf-shaped Koch fractal with a modified CPW-fed antenna. International Journal of Electronics Letters 2018; 6 (2): 137—145. doi:10.1080/21681724.2017.1329942

[38] Abolade JO, Konditi DB, Dharmadhikary VM. Bio-inspired wideband antenna for wireless applications based on perturbation technique. Heliyon 2020; 6 (7) :e04282. doi:10.1016/j.heliyon.2020.e04282

[39] Çelik K, Kurt E. Design and implementation of a dual band bioinspired leaf rectenna for RF energy harvesting applications. International Journal of RF and Microwave Computer-Aided Engineering 2021; 31 (11): e22868. doi:10.1002/mmce.22868

[40] Vaccaro S, Mosig JR, de Maagt P. Two advanced solar antenna "SOLANT" designs for satellite and terrestrial communications. IEEE Transactions on Antennas and Propagation 2003; 51 (8) :2028—2034. doi:10.1109/TAP.2003.815424

[41] Georgiadis A, Collado A, Via S, Meneses C. Flexible hybrid solar/EM energy harvester for autonomous sensors. 2011 IEEE MTT-S International Microwave Symposium; Baltimore, Maryland, USA; 2011. pp.1—4. doi: 10.1109/MWSYM.2011.5972963

[42] Collado A, Georgiadis A. Conformal hybrid solar and electromagnetic (EM) energy harvesting rectenna. IEEE Transactions on Circuits and Systems I: Regular Papers 2013; 60 (8): 2225—2234. doi:10.1109/TCSI.2013.2239154

[43] Bito J, Bahr R, Hester JG, Nauroze SA, Georgiadis A et al. A novel solar and electromagnetic energy harvesting system with a 3-D printed package for energy efficient Internet-of-Things wireless sensors. IEEE Transactions on Microwave Theory and Techniques 2017; 65 (5): 1831—1842. doi:10.1109/TMTT.2017.2660487

[44] Zhang Y, Shen S, Chiu CY, Murch R. Hybrid RF-solar energy harvesting systems utilizing transparent multiport micromeshed antennas. IEEE Transactions on Microwave Theory and Techniques 2019; 67 (11): 4534—4546. doi:10.1109/TMTT.2019.2930507

[45] Ray KP, Anob PV, Kapur R, Kumar G. Broadband planar rectangular monopole antennas. Microwave and Optical Technology Letters 2001; 28 (1): 55—59. doi:10.1002/1098-2760(20010105)28:1<55::AID-MOP16>3.0.CO;2-X

[46] Sugumaran B, Balasubramanian R, Palaniswamy SK. Reduced specific absorption rate compact flexible monopole antenna system for smart wearable wireless communications. Engineering Science and Technology, an International Journal 2021. 24 (3) :682—693. doi:10.1016/j.jestch.2020.12.012

[47] Farahani M, Mohammad-Ali-Nezhad S. A novel UWB printed monopole MIMO antenna with non-uniform transmission line using nonlinear model predictive. Engineering Science and Technology, an International Journal 2020; 23 (6) :1385—1396. doi:10.1016/j.jestch.2020.05.006

[48] Kumar G, Ray KP. Broadband Microstrip Antennas. Artech house, 2003.

[49] Karthikeyan M, Sitharthan R, Ali T, Roy B. Compact multiband CPW fed monopole antenna with square ring and T-shaped strips. Microwave and Optical Technology Letters 2020; 62 (2) :926—932. doi:10.1002/mop.32106

[50] Azarm B, Ghobadi C, Nourinia J, Abbasilayegh M, Karamirad M. A Band-Notched Square Monopole Antenna designed for Bandwidth Enhancement in UWB Applications. Applied Computational Electromagnetics Society Journal 2017; 32 (10).

[51] Bhatia SS, Sivia JS. A novel design of circular monopole antenna for wireless applications. Wireless Personal Communications 2016; 91 (3) :1153—1161. doi:10.1007/s11277-016-3518-z

[52] ElMahgoub K. Slotted triangular monopole antenna for UHF RFID readers. Applied Computational Electromagnetics Society Journal 2016; 1 (1) :24-27.

[53] Naik KK, Gopi D. Flexible CPW-fed split-triangular shaped patch antenna for WiMAX applications. Progress In Electromagnetics Research M 2018;70: 157—166. doi:10.2528/PIERM18060304

[54] Çelik, F. A Survey on the Properties of Microstrip Antennas with Different Shapes. Transactions On Electromagnetic Spectrum, 2022; 1(1), 5–9. https://doi.org/10.5281/zenodo.6643748

[55] Ak, H. H. On-Body Monopole Antenna Design and Analyses for the UWB Applications. Transactions On Electromagnetic Spectrum, 2022; 1(1), 19–23. https://doi.org/10.5281/zenodo.6646264

[56] Ray KP, Ranga Y. Printed rectangular monopole antennas. 2006 IEEE Antennas and Propagation Society International Symposium. Albuquerque, New Mexico; 2006. pp. 1693—1696. doi: 10.1109/APS.2006.1710888

[57] Chaudhary P, Kumar A. Compact ultra-wideband circularly polarized CPW-fed monopole antenna. AEU-International Journal of Electronics and Communications 2019;107: 137—145. doi:10.1016/j.aeue.2019.05.025

[58] Yadav D, Abegaonkar MP, Koul SK, Tiwari V, Vivekanand B et al. A compact dual band-notched UWB circular monopole antenna with parasitic resonators. AEU-International Journal of Electronics and Communications 2018; 84: 313—320. doi:10.1016/j.aeue.2017.12.020

[59] Piñuela M, Mitcheson PD, Lucyszyn S. Ambient RF energy harvesting in urban and semi-urban environments. IEEE Transactions on microwave theory and techniques 2013; 61 (7) : 2715—2726. doi:10.1109/TMTT.2013.2262687

[60] Sun H, Guo YX, He M, Zhong Z. Design of a high-efficiency 2.45-GHz rectenna for low-input-power energy harvesting. IEEE Antennas and Wireless Propagation Letters 2012; 11:929-932. doi:10.1109/LAWP.2012.2212232

[61] Lin QW, Zhang XY. Differential rectifier using resistance compression network for improving efficiency over extended input power range. IEEE Transactions on Microwave Theory and Techniques 2016; 64 (9): 2943—2954. doi:10.1109/TMTT.2016.2592531

[62] Olgun U, Chen CC, Volakis JL. Investigation of rectenna array configurations for enhanced RF power harvesting. IEEE antennas and wireless propagation letters 2011; 10: 262—265. doi:10.1109/LAWP.2011.2136371

[63] Chen YS, Chiu CW. Maximum achievable power conversion efficiency obtained through an optimized rectenna structure for RF energy harvesting. IEEE Transactions on Antennas and Propagation 2017; 65 (5) : 2305—2317. doi:10.1109/TAP.2017.2682228

[64] Niotaki K, Giuppi F, Georgiadis A, Collado A. Solar/EM energy harvester for autonomous operation of a monitoring sensor platform. Wireless Power Transfer 2014; 1 (1) : 44. doi:10.1017/wpt.2014.6